Monthly Notices
of the
ROYAL ASTRONOMICAL SOCIETY

Mon. Not. R. Astron. Soc. **417,** 1559–1575 (2011) doi:10.1111/j.1365-2966.2011.18627.x

Washington photometry of 14 intermediate-age to old star clusters in the Small Magellanic Cloud

Andrés E. Piatti,[1⋆] Juan J. Clariá,[2] Eduardo Bica,[3] Doug Geisler,[4] Andrea V. Ahumada[2,5] and Léo Girardi[6]

[1]*Instituto de Astronomía y Física del Espacio, CC 67, Suc. 28, 1428 Capital Federal, Argentina*
[2]*Observatorio Astronómico, Laprida 854, 5000 Córdoba, Argentina*
[3]*Depto. de Astronomía, Universidade Federal do Rio Grande do Sul, CP 15051, Porto Alegre 91500-970, Brazil*
[4]*Departamento de Física, Universidad de Concepción, Casilla 160-C, Concepción, Chile*
[5]*European Southern Observatory, Alonso de Córdova 3107, Santiago, Chile*
[6]*Osservatorio Astronomico di Padova INAF, Vicolo dell'Osservatorio 5, I-35122 Padova, Italy*

Accepted 2011 March 1. Received 2011 February 21; in original form 2010 December 17

ABSTRACT

We present CCD photometry in the Washington system C, T_1 and T_2 passbands down to $T_1 \sim 23$ in the fields of L3, L28, HW 66, L100, HW 79, IC 1708, L106, L108, L109, NGC 643, L112, HW 84, HW 85 and HW 86, 14 Small Magellanic Cloud (SMC) clusters, most of them poorly studied objects. We measured T_1 magnitudes and $C - T_1$ and $T_1 - T_2$ colours for a total of 213 516 stars spread throughout cluster areas of 14.7×14.7 arcmin^2 each. We carried out an in-depth analysis of the field star contamination of the colour–magnitude diagrams (CMDs) and statistically cleaned the cluster CMDs. Based on the best fits of isochrones computed by the Padova group to the (T_1, $C - T_1$) CMDs, as well as from the $\delta(T_1)$ index and the standard giant branch procedure, we derived ages and metallicities for the cluster sample. With the exception of IC 1708, a relatively metal-poor Hyades-age cluster, the remaining 13 objects are between intermediate and old age (from 1.0 to 6.3 Gyr), their [Fe/H] values ranging from −1.4 to −0.7 dex. By combining these results with others available in the literature, we compiled a sample of 43 well-known SMC clusters older than 1 Gyr, with which we produced a revised age distribution. We found that the present clusters' age distribution reveals two primary excesses of clusters at $t \sim 2$ and 5 Gyr, which engraves the SMC with clear signs of enhanced formation episodes at both ages. In addition, we found that from the birth of the SMC cluster system until approximately the first 4 Gyr of its lifetime, the cluster formation resembles that of a constant formation rate scenario.

Key words: techniques: photometric – galaxies: individual: SMC – Magellanic Clouds – galaxies: star clusters: general.

1 INTRODUCTION

The Small Magellanic Cloud (SMC) has long been recognized as a fundamental benchmark for a wide variety of astrophysical studies. As one of the closest star-forming dwarf irregular galaxies, it is the ideal local analogue for the detailed study of these most common and primeval galaxies. It is also an excellent laboratory for the exploration of the role of key parameters, such as age and metallicity, in a number of contexts like star formation, initial mass function, stellar and galaxy evolution, etc. In addition, the current cold dark matter (CDM) paradigm of galaxy formation suggests that massive galaxy spheroids, such as the Milky Way (MW) halo, are formed by the accretion/merger of smaller, satellite galaxies (Searle & Zinn 1978; Zentner & Bullock 2003).

Models suggest that the majority of the MW building blocks were very massive and were assimilated very early in its history (Sales et al. 2007). The models also suggest that existing low-mass galaxies like the SMC are survivors of this assimilation process and thus underwent a different chemical evolution (Robertson et al. 2005). Finally, many dynamical simulations (e.g. Bekki et al. 2004) suggest that the MW, Large Magellanic Cloud (LMC) and SMC constitute a long-term interacting system. Possible close encounters in the last few Gyr may well have stimulated star formation on a global scale in both the SMC and LMC (Murai & Fujimoto 1980; Gardiner, Sawa & Fujimoto 1994; Bekki et al. 2004). However, the most recent proper motion values of the Magellanic Clouds (MCs) suggest that they are unbound from each other and only just

⋆E-mail: andres@iafe.uba.ar

beginning their first close encounter with the MW (Kallivayalil et al. 2006; Piatek, Pryor & Olszewski 2008).

As most SMC stars may have formed in clusters (Chiosi et al. 2006, but see Bastian et al. 2009 for an opposing view), their study is especially relevant to explore the structure, kinematics, star formation and chemical evolution history of this galaxy. SMC star clusters are also of utmost importance for the study of stellar populations in distant galaxies, since they cover age and abundance space that is not occupied by their galactic counterparts. In addition, while the LMC cluster system suffers from the well-known age gap (Da Costa 1991; Geisler et al. 1997), the SMC holds clusters that have formed more or less continuously over the past 11 Gyr (e.g. Glatt et al. 2008b). Indeed, the SMC is the only known dwarf galaxy in the Local Group that has formed and preserved populous star clusters through most of the age of the Universe, the SMC having been prolific in cluster production. Hodge (1986) estimated the SMC to have some 2000 clusters. Therefore, such clusters are ideal tracers of the global and specific details of the SMC evolution, with the only exception of NGC 121, not only the oldest cluster known but also the only true globular cluster in the SMC which is only 11 Gyr old (Glatt et al. 2008a). So we must turn to other tracers to unravel the earliest epochs. Bica & Schmitt (1995) and Bica et al. (1999) updated the SMC and LMC catalogues to 554 and 2577 clusters, respectively. In the former study, the Bica–Schmitt (BS) clusters were discovered. Some of them turned out to be rather prominent clusters projected on to the main body and outer parts of the SMC (Section 5). More recently, Bica et al. (2008a) catalogued 3740 clusters in both clouds, this number amounting to ≈60 per cent of the total of Hodge's estimate in both clouds. Probably, those expectations will be fulfilled by the Vista Magellanic Cloud (VMC) survey.[1] VMC's homogeneous deeper view of the MCs will soon be available in the Y, J and K_s bands (e.g. Kerber et al. 2009; Cioni et al. 2011). We estimated ages and metallicities for MC clusters with the accuracy of the Washington photometry (e.g. Piatti et al. 2008 for the SMC; Piatti et al. 2011 for the LMC). The present sample of intermediate-age and old SMC clusters, together with the above estimated results, will certainly play a role as reference parameters for VMC studies. These clusters and fields are conveniently distributed across the Magellanic System.

Despite their utility and unique advantages, SMC clusters have been surprisingly underexploited. The number of SMC clusters with well-determined ages from deep main-sequence (MS) photometry is minimal. Thus, the really detailed information, viz. accurate ages, abundances and velocities, necessary to fully utilize SMC clusters, both as tracers of SMC formation and chemical and dynamical evolution history and as templates for studying stellar populations in more distant galaxies, is sorely lacking. Our group has begun trying to solve this deficit by observing a large sample of SMC clusters.

This paper is organized as follows. Section 2 describes observations and data reduction. Section 3 focuses on describing the main features of the colour–magnitude diagrams (CMDs) and the method applied to minimize field star contamination. In this section, we also show how cluster sizes are determined from their stellar density profiles. Reddenings, ages and metallicities for the 14 selected clusters are derived in Section 4, while the analysis and discussion of the results is presented in Section 5, together with a thorough discussion of the age distribution of SMC star clusters older than 1 Gyr. Our main findings are summarized in Section 6.

[1] http://star.herts.ac.uk/~mcioni/vmc/

2 OBSERVATIONS AND REDUCTION

We obtained images for the cluster sample on the nights of 2000 October 29–31, with a 2048 × 2048 pixel Tektronix CCD attached to the 1.5-m telescope (scale 0.432 arcsec pixel^{-1}) at Cerro Tololo Inter-American Observatory (CTIO), Chile. Its field of view is 14.7 × 14.7 arcmin^2. We used the Washington C (Canterna 1976) and Kron–Cousins R and I filters in order to keep consistent with our previous studies. The R filter has a significantly higher throughput as compared with the standard Washington T_1 filter so that R magnitudes can be accurately transformed to yield T_1 magnitudes (Geisler 1996). A series of bias and dome and sky flat-field exposures per filter were obtained to calibrate the CCD instrumental signature. Table 1 shows the log of the observations with filters, exposure times, airmasses and seeing estimates. A large number (typically 20) of standard stars from the list of Geisler (1996) were also observed on the last night. Care was taken to cover a wide colour and airmass range for these standards in order to bracket and calibrate the programme stars properly observed on that night. Shorter exposures were obtained for the programme clusters on the same night and longer ones during the first two nights.

We applied bias subtraction to all the images and flat-fielding to both standard and programme field images, using weighted combined signal-calibrator frames and standard observational techniques and tasks in IRAF.[2] The resulting processed images turned out to be satisfactorily flat. We then derived the instrumental magnitudes for the standard stars from aperture photometry using DAOPHOT/IRAF routines (Stetson, Davis & Crabtree 1990). We obtained, through least-squares fits, the following mean transformation equations between instrumental and standard magnitudes for the third night:

$$c = (1.013 \pm 0.016) + T_1 + (C - T_1) + (0.324 \pm 0.010)X_C - (0.062 \pm 0.012)(C - T_1), \quad (1)$$

$$r = (0.712 \pm 0.011) + T_1 + (0.084 \pm 0.004)X_{T_1} - (0.014 \pm 0.007)(C - T_1), \quad (2)$$

$$i = (1.596 \pm 0.037) + T_2 + (0.041 \pm 0.024)X_{T_2} - (0.040 \pm 0.035)(T_1 - T_2), \quad (3)$$

where X represents the effective airmass and capital and lowercase letters stand for standard and instrumental magnitudes, respectively. The coefficients were derived through the IRAF routine FITPARAM, yielding rms errors of 0.015 for c, 0.012 for r and 0.022 for i, which indicates that the night was indeed photometric.

The stellar photometry was performed using the star finding and point spread function (PSF) fitting routines in the DAOPHOT/ALLSTAR suite of programs (Stetson et al. 1990). For each frame, a quadratically varying PSF was derived by fitting ∼100 stars, once the neighbours were eliminated using a preliminary PSF derived from the brightest, least contaminated 35–40 stars. Both groups of PSF stars were interactively selected. We then used the ALLSTAR program to apply the resulting PSF to the identified stellar objects and to create a subtracted image which was used to find and measure magnitudes of additional fainter stars. This procedure was repeated three times for each frame. Finally, we computed aperture corrections from the comparison of PSF and aperture

[2] IRAF is distributed by the National Optical Astronomy Observatories, which is operated by the Association of Universities for Research in Astronomy, Inc., under contract with the National Science Foundation.

Table 1. Observation log of selected clusters.

Star cluster[a]	α_{2000} ($^{h}\,^{m}\,^{s}$)	δ_{2000} ($^{\circ}\,'\,''$)	l ($^{\circ}$)	b ($^{\circ}$)	Date	Filter	Exposure (s)	Airmass	Seeing (arcsec)
L3, ESO 28−SC13	0 18 25	−74 19 07	305.95	−42.61	2000 October 29	*C*	1800	1.44	1.8
						R	600	1.46	1.5
						I	600	1.45	1.1
					2000 October 31	*C*	180	1.43	1.9
						R	60	1.44	1.4
						I	60	1.44	1.9
L28	0 42 59	−72 35 19	303.82	−44.52	2000 October 29	*C*	1800	1.37	2.1
						R	600	1.39	1.8
						I	600	1.38	1.8
					2000 October 31	*C*	180	1.42	2.1
						R	60	1.41	1.5
						I	60	1.41	1.5
HW 66, ESO 29−SC36	1 12 04	−75 11 51	301.16	−41.86	2000 October 30	*C*	1800	1.41	2.3
						R	600	1.44	1.7
						I	600	1.45	2.3
					2000 October 31	*C*	180	1.44	2.1
						R	60	1.44	1.5
						I	60	1.44	1.9
L100, ESO 51−SC27	1 18 16	−72 00 06	300.01	−44.97	2000 October 29	*C*	1800	1.36	1.9
						R	600	1.34	1.7
						I	600	1.33	1.3
					2000 October 31	*C*	180	1.37	1.9
						R	60	1.36	1.7
						I	60	1.36	2.1
HW 79	1 22 48	−75 00 06	300.21	−41.96	2000 October 29	*C*	1800	1.41	2.0
						R	600	1.40	1.8
						I	600	1.41	1.5
					2000 October 31	*C*	180	1.42	2.0
						R	60	1.43	2.0
						I	60	1.42	2.0
IC 1708, L102, ESO 52−SC2	1 24 56	−71 11 01	299.08	−45.69	2000 October 30	*C*	1800	1.33	2.0
						R	600	1.32	1.8
						I	600	1.32	2.1
					2000 October 31	*C*	180	1.34	1.9
						R	60	1.33	1.3
						I	60	1.33	1.7
L106, ESO 29−SC44	1 30 38	−76 03 16	299.82	−40.84	2000 October 31	*C*	180	1.44	2.0
						R	60	1.44	1.2
						I	60	1.44	1.5
L108	1 31 32	−71 57 10	298.57	−44.83	2000 October 29	*C*	1800	1.36	1.8
						R	600	1.40	2.0
						I	600	1.38	1.5
					2000 October 31	*C*	180	1.34	1.7
						R	60	1.34	1.3
						I	60	1.34	1.2
L109, ESO 29−SC46	1 33 14	−74 10 02	299.07	−42.65	2000 October 30	*C*	1800	1.43	2.0
						R	600	1.41	1.8
						I	600	1.42	1.8
					2000 October 31	*C*	180	1.39	1.9
						R	60	1.39	1.4
						I	60	1.39	1.7
NGC 643, L111, ESO 29−SC50	1 35 00	−75 33 24	299.34	−41.27	2000 October 31	*C*	180	1.42	1.6
						R	60	1.42	1.4
						I	60	1.42	1.4
L112	1 35 58	−75 27 28	299.23	−41.35	2000 October 31	*C*	180	1.42	1.6
						R	60	1.42	1.4
						I	60	1.42	1.4
HW 84	1 41 28	−71 09 58	297.22	−45.40	2000 October 30	*C*	1800	1.42	2.0
						R	600	1.48	2.1
						I	600	1.40	2.1
					2000 October 31	*C*	180	1.33	2.0
						R	60	1.33	2.0
						I	60	1.33	2.2

Table 1 – *continued*

Star cluster[a]	α_{2000} ($^{h}\,^{m}\,^{s}$)	δ_{2000} ($^{\circ}\,'\,''$)	l ($^{\circ}$)	b ($^{\circ}$)	Date	Filter	Exposure (s)	Airmass	Seeing (arcsec)
HW 85	1 42 36	−71 16 53	297.14	−45.27	2000 October 30	*C*	1800	1.42	2.0
						R	600	1.48	2.1
						I	600	1.40	2.1
					2000 October 31	*C*	180	1.33	2.0
						R	60	1.33	2.0
						I	60	1.33	2.2
HW 86	1 42 22	−74 10 24	298.26	−42.49	2000 October 31	*C*	1800	1.41	1.8
						R	600	1.45	1.5
						I	600	1.43	1.3

[a]Cluster identifications are from Lindsay (1958, L), Hodge & Wright (1974, HW) and Lauberts (1982, ESO).

Table 2. CCD CT_1T_2 data of stars in the field of L3. This is a sample of the full table, which is available with the online version of the article (see Supporting Information).

Star	X (pixel)	Y (pixel)	T_1 (mag)	$\sigma(T_1)$ (mag)	n_{T_1}	$C-T_1$ (mag)	$\sigma(C-T_1)$ (mag)	n_{C-T_1}	T_1-T_2 (mag)	$\sigma(T_1-T_2)$ (mag)	$n_{T_1-T_2}$
–	–	–	–	–	–	–	–	–	–	–	–
4466	827.070	625.486	19.263	0.005	2	1.425	0.063	2	0.474	0.009	2
4467	707.085	625.500	19.311	0.011	2	1.248	0.013	2	0.410	0.038	2
4468	1292.357	625.647	20.516	0.013	2	1.356	0.119	2	0.556	0.102	1
–	–	–	–	–	–	–	–	–	–	–	–

Table 3. CCD CT_1T_2 data of stars in the field of L28. This is a sample of the full table, which is available with the online version of the article (see Supporting Information).

Star	X (pixel)	Y (pixel)	T_1 (mag)	$\sigma(T_1)$ (mag)	n_{T_1}	$C-T_1$ (mag)	$\sigma(C-T_1)$ (mag)	n_{C-T_1}	T_1-T_2 (mag)	$\sigma(T_1-T_2)$ (mag)	$n_{T_1-T_2}$
–	–	–	–	–	–	–	–	–	–	–	–
368	447.421	5.620	18.995	0.017	1	1.258	0.033	1	0.471	0.024	1
369	2005.356	5.634	20.734	0.106	2	0.115	0.423	2	0.168	0.099	1
370	682.912	5.635	19.057	0.029	1	1.556	0.058	1	0.312	0.071	1
–	–	–	–	–	–	–	–	–	–	–	–

Table 4. CCD CT_1T_2 data of stars in the field of HW 66. This is a sample of the full table, which is available with the online version of the article (see Supporting Information).

Star	X (pixel)	Y (pixel)	T_1 (mag)	$\sigma(T_1)$ (mag)	n_{T_1}	$C-T_1$ (mag)	$\sigma(C-T_1)$ (mag)	n_{C-T_1}	T_1-T_2 (mag)	$\sigma(T_1-T_2)$ (mag)	$n_{T_1-T_2}$
–	–	–	–	–	–	–	–	–	–	–	–
153	1332.922	78.477	18.998	0.028	1	1.138	0.042	1	0.494	0.056	1
154	824.433	79.000	19.151	0.029	1	1.433	0.050	1	0.472	0.054	1
155	799.937	79.526	17.526	0.010	1	1.429	0.018	1	0.483	0.017	1
–	–	–	–	–	–	–	–	–	–	–	–

magnitudes by using the neighbour-subtracted PSF star sample. The resulting aperture corrections were on average less than 0.02 mag (absolute value) for *c*, *r* and *i* images, respectively (Piatti et al. 1999).

The resulting instrumental magnitudes for the clusters observed during that night were standardized using equations (1) to (3) which, in turn, were used to calibrate the instrumental photometry obtained for the first two nights. We combined all the independent measurements using the standalone DAOMATCH and DAOMASTER programs, kindly provided by Peter Stetson. The final information gathered for each cluster consists of a running number per star of the x and y coordinates, of the measured T_1 magnitudes and $C-T_1$ and T_1-T_2 colours, of the observational errors $\sigma(T_1)$, $\sigma(C-T_1)$ and $\sigma(T_1-T_2)$ and of the number of observations per filter. We adopted the photometric errors provided by ALLSTAR[3] for stars with only one measure. Tables 2–15 give this information for L3, L28, HW 66, L100, HW 79, IC 1708, L106, L108, L109,

[3] Program kindly provided by P. B. Stetson.

Table 5. CCD CT_1T_2 data of stars in the field of L100. This is a sample of the full table, which is available with the online version of the article (see Supporting Information).

Star	X (pixel)	Y (pixel)	T_1 (mag)	$\sigma(T_1)$ (mag)	n_{T_1}	$C-T_1$ (mag)	$\sigma(C-T_1)$ (mag)	n_{C-T_1}	T_1-T_2 (mag)	$\sigma(T_1-T_2)$ (mag)	$n_{T_1-T_2}$
–	–	–	–	–	–	–	–	–	–	–	–
12	756.629	3.481	18.867	0.022	1	1.391	0.037	1	0.457	0.049	1
13	659.685	3.880	15.395	0.021	1	0.880	0.022	1	0.352	0.023	1
14	1358.203	4.535	19.509	0.024	1	1.980	0.092	1	0.550	0.064	1
–	–	–	–	–	–	–	–	–	–	–	–

Table 6. CCD CT_1T_2 data of stars in the field of HW 79. This is a sample of the full table, which is available with the online version of the article (see Supporting Information).

Star	X (pixel)	Y (pixel)	T_1 (mag)	$\sigma(T_1)$ (mag)	n_{T_1}	$C-T_1$ (mag)	$\sigma(C-T_1)$ (mag)	n_{C-T_1}	T_1-T_2 (mag)	$\sigma(T_1-T_2)$ (mag)	$n_{T_1-T_2}$
–	–	–	–	–	–	–	–	–	–	–	–
212	677.871	52.479	22.152	0.141	1	1.090	0.174	1	−0.560	0.534	1
213	1494.161	52.658	22.119	0.151	1	0.828	0.171	1	99.999	9.999	0
214	704.511	52.734	18.198	0.017	2	1.663	0.016	2	0.490	0.029	2
–	–	–	–	–	–	–	–	–	–	–	–

Table 7. CCD CT_1T_2 data of stars in the field of IC 1708. This is a sample of the full table, which is available with the online version of the article (see Supporting Information).

Star	X (pixel)	Y (pixel)	T_1 (mag)	$\sigma(T_1)$ (mag)	n_{T_1}	$C-T_1$ (mag)	$\sigma(C-T_1)$ (mag)	n_{C-T_1}	T_1-T_2 (mag)	$\sigma(T_1-T_2)$ (mag)	$n_{T_1-T_2}$
–	–	–	–	–	–	–	–	–	–	–	–
875	620.049	163.605	21.646	0.745	2	0.495	0.110	1	1.028	0.803	2
876	672.379	163.850	18.611	0.002	2	1.225	0.000	2	0.392	0.039	1
877	1595.278	164.219	19.096	0.005	2	1.507	0.047	2	0.434	0.027	2
–	–	–	–	–	–	–	–	–	–	–	–

Table 8. CCD CT_1T_2 data of stars in the field of L106. This is a sample of the full table, which is available with the online version of the article (see Supporting Information).

Star	X (pixel)	Y (pixel)	T_1 (mag)	$\sigma(T_1)$ (mag)	n_{T_1}	$C-T_1$ (mag)	$\sigma(C-T_1)$ (mag)	n_{C-T_1}	T_1-T_2 (mag)	$\sigma(T_1-T_2)$ (mag)	$n_{T_1-T_2}$
–	–	–	–	–	–	–	–	–	–	–	–
950	426.682	436.214	21.531	0.112	1	99.999	9.999	0	2.063	0.164	1
951	249.963	436.714	18.485	0.026	1	−0.415	0.028	1	−0.076	0.043	1
952	1108.099	437.885	19.166	0.024	1	1.295	0.042	1	0.547	0.055	1
–	–	–	–	–	–	–	–	–	–	–	–

Table 9. CCD CT_1T_2 data of stars in the field of L108. This is a sample of the full table, which is available with the online version of the article (see Supporting Information).

Star	X (pixel)	Y (pixel)	T_1 (mag)	$\sigma(T_1)$ (mag)	n_{T_1}	$C-T_1$ (mag)	$\sigma(C-T_1)$ (mag)	n_{C-T_1}	T_1-T_2 (mag)	$\sigma(T_1-T_2)$ (mag)	$n_{T_1-T_2}$
–	–	–	–	–	–	–	–	–	–	–	–
222	253.725	31.179	22.144	0.100	1	0.691	0.118	1	0.570	0.172	1
223	383.727	31.231	16.226	0.014	2	2.553	0.056	2	0.640	0.051	2
224	794.436	31.270	17.577	0.001	2	1.628	0.001	2	−1.460	0.193	1
–	–	–	–	–	–	–	–	–	–	–	–

NGC 643, L112, HW 84, HW 85 and HW 86, respectively. Only a portion of these tables is shown here for guidance regarding their form and content. The whole content of Tables 2–15 is available with the online version of the article (see Supporting Information).

We first examined the quality of our photometry in order to evaluate the influence of the photometric errors on the cluster fiducial characteristics in the CMDs. The behaviour of $\sigma(T_1)$, $\sigma(C-T_1)$ and $\sigma(T_1-T_2)$ as a function of T_1 is shown in Table 16. From this

Table 10. CCD CT_1T_2 data of stars in the field of L109. This is a sample of the full table, which is available with the online version of the article (see Supporting Information).

Star	X (pixel)	Y (pixel)	T_1 (mag)	$\sigma(T_1)$ (mag)	n_{T_1}	$C-T_1$ (mag)	$\sigma(C-T_1)$ (mag)	n_{C-T_1}	T_1-T_2 (mag)	$\sigma(T_1-T_2)$ (mag)	$n_{T_1-T_2}$
–	–	–	–	–	–	–	–	–	–	–	–
773	1587.654	167.545	19.209	0.042	2	1.493	0.094	2	0.493	0.012	2
774	726.423	168.025	21.077	0.553	2	2.080	0.204	1	1.178	0.927	2
775	1659.693	168.202	14.427	0.014	2	1.350	0.011	2	0.367	0.017	2
–	–	–	–	–	–	–	–	–	–	–	–

Table 11. CCD CT_1T_2 data of stars in the field of NGC 643. This is a sample of the full table, which is available with the online version of the article (see Supporting Information).

Star	X (pixel)	Y (pixel)	T_1 (mag)	$\sigma(T_1)$ (mag)	n_{T_1}	$C-T_1$ (mag)	$\sigma(C-T_1)$ (mag)	n_{C-T_1}	T_1-T_2 (mag)	$\sigma(T_1-T_2)$ (mag)	$n_{T_1-T_2}$
–	–	–	–	–	–	–	–	–	–	–	–
1453	1873.006	814.746	14.009	0.009	1	1.287	0.009	1	0.384	0.011	1
1454	1749.132	815.569	13.918	0.008	1	1.143	0.008	1	0.402	0.011	1
1455	1974.151	815.939	21.023	0.101	1	1.187	0.193	1	99.999	9.999	0
–	–	–	–	–	–	–	–	–	–	–	–

Table 12. CCD CT_1T_2 data of stars in the field of L112. This is a sample of the full table, which is available with the online version of the article (see Supporting Information).

Star	X (pixel)	Y (pixel)	T_1 (mag)	$\sigma(T_1)$ (mag)	n_{T_1}	$C-T_1$ (mag)	$\sigma(C-T_1)$ (mag)	n_{C-T_1}	T_1-T_2 (mag)	$\sigma(T_1-T_2)$ (mag)	$n_{T_1-T_2}$
–	–	–	–	–	–	–	–	–	–	–	–
1701	1689.255	1021.031	15.409	0.009	1	2.299	0.012	1	0.639	0.016	1
1702	1458.040	1021.295	16.861	0.013	1	1.680	0.054	1	0.516	0.019	1
1703	654.632	1021.480	19.079	0.028	1	1.350	0.040	1	0.465	0.049	1
–	–	–	–	–	–	–	–	–	–	–	–

Table 13. CCD CT_1T_2 data of stars in the field of HW 84. This is a sample of the full table, which is available with the online version of the article (see Supporting Information).

Star	X (pixel)	Y (pixel)	T_1 (mag)	$\sigma(T_1)$ (mag)	n_{T_1}	$C-T_1$ (mag)	$\sigma(C-T_1)$ (mag)	n_{C-T_1}	T_1-T_2 (mag)	$\sigma(T_1-T_2)$ (mag)	$n_{T_1-T_2}$
–	–	–	–	–	–	–	–	–	–	–	–
82	73.724	17.023	22.356	0.623	2	0.061	0.305	1	1.815	0.223	1
83	29.553	17.107	21.444	0.027	2	0.425	0.000	2	0.132	0.231	1
84	1075.269	17.242	18.326	0.021	2	1.616	0.016	2	0.443	0.106	2
–	–	–	–	–	–	–	–	–	–	–	–

Table 14. CCD CT_1T_2 data of stars in the field of HW 85. This is a sample of the full table, which is available with the online version of the article (see Supporting Information).

Star	X (pixel)	Y (pixel)	T_1 (mag)	$\sigma(T_1)$ (mag)	n_{T_1}	$C-T_1$ (mag)	$\sigma(C-T_1)$ (mag)	n_{C-T_1}	T_1-T_2 (mag)	$\sigma(T_1-T_2)$ (mag)	$n_{T_1-T_2}$
–	–	–	–	–	–	–	–	–	–	–	–
550	1091.735	167.417	21.327	0.566	2	1.823	0.118	1	0.632	0.084	1
551	2003.567	167.547	20.561	0.087	2	2.006	0.277	2	0.605	0.113	2
552	236.360	167.749	18.290	0.009	2	1.447	0.005	2	0.433	0.036	2
–	–	–	–	–	–	–	–	–	–	–	–

table we conclude that we could detect and measure the turn-off (TO) for the present cluster sample – which was used in our age estimates – with an uncertainty of ≈0.20 mag. Moreover, by using the theoretical isochrones of Girardi et al. (2002) and the SMC distance modulus, we concluded that the faintest observed MS field stars correspond to TOs for stellar populations as old as 5 ± 1 Gyr ($T_1 \approx 22.0 \pm 0.3$ mag). Slightly fainter TOs can be reached at the expense of larger errors. Table 17 presents the results of the

Table 15. CCD CT_1T_2 data of stars in the field of HW 86. This is a sample of the full table, which is available with the online version of the article (see Supporting Information).

Star	X (pixel)	Y (pixel)	T_1 (mag)	$\sigma(T_1)$ (mag)	n_{T_1}	$C-T_1$ (mag)	$\sigma(C-T_1)$ (mag)	n_{C-T_1}	T_1-T_2 (mag)	$\sigma(T_1-T_2)$ (mag)	$n_{T_1-T_2}$
–	–	–	–	–	–	–	–	–	–	–	–
64	1687.991	15.863	21.684	0.117	1	1.303	0.153	1	−0.342	0.218	1
65	7.398	16.112	21.100	0.094	1	1.737	0.143	1	−0.256	0.177	1
66	1399.266	16.176	19.301	0.019	1	0.405	0.022	1	−0.739	0.045	1
–	–	–	–	–	–	–	–	–	–	–	–

Table 16. Magnitude and colour photometric errors as a function of T_1.

ΔT_1 (mag)	$\sigma(T_1)$ (mag)	$\sigma(C-T_1)$ (mag)	$\sigma(T_1-T_2)$ (mag)
14–15	0.015–0.030	0.020–0.040	0.020–0.040
15–16	0.015–0.030	0.020–0.040	0.020–0.040
16–17	0.015–0.030	0.020–0.040	0.020–0.040
17–18	0.015–0.030	0.020–0.040	0.020–0.040
18–19	0.040	0.050	0.060
19–20	0.070	0.090	0.100
20–21	0.130	0.170	0.180
21–22	0.200	0.250	0.30
22–23	0.300	0.350	–

Table 17. Comparison of the present photometric data with previous ones.

Name	$\Delta(T_1)$	$\Delta(C-T_1)$	n	Ref.[a]
L108	0.039 ± 0.082	-0.022 ± 0.097	1884	1
L112	0.034 ± 0.066	0.020 ± 0.088	268	2

[a]1 – Piatti et al. (2007a); 2 – Piatti et al. (2007b).

comparison between the photometry by Piatti et al. (2007c, L108) and Piatti et al. (2007b, L112) and ours, measured by the differences $\Delta T_1 = T_{1_{\rm pub}} - T_{1_{\rm our}}$ and $\Delta(C-T_1) = (C-T_1)_{\rm pub} - (C-T_1)_{\rm our}$, which were computed for the number n of common stars. It can be seen that the agreement is excellent, T_1 magnitudes being $\sim$1.5 mag fainter than their respective photometric limits. We would like to point out that the $T_1 - T_2$ colours are presented here only for completeness purposes and are intended to be used in a forthcoming paper.

3 ANALYSIS OF THE COLOUR–MAGNITUDE DIAGRAMS

In Fig. 1 we show – as an example – the CMD of all the measured stars in the field of L28, which is the most populated observed field (92 771 stars). The remaining cluster fields exhibit CMDs with fairly similar characteristics. A mixture of young and old stellar populations clearly appears to be the main SMC feature of the CMDs. The most obvious traits are the long MS which extends approximately 5 mag in T_1, the populous and broad subgiant branch – an indicator of the evolution of stars with ages (masses) within a non-negligible range – the red clump (RC) and the red giant branch (RGB). The RC is somewhat elongated in T_1 and appears to be populated at brighter magnitudes by the so-called 'vertical red clump' structure (Zaritsky & Lin 1997; Gallart 1998; Ibata, Lewis & Beaulieu 1998). However, there is no clear existing evidence of the vertical structure stars seen in some LMC fields (Piatti et al. 1999).

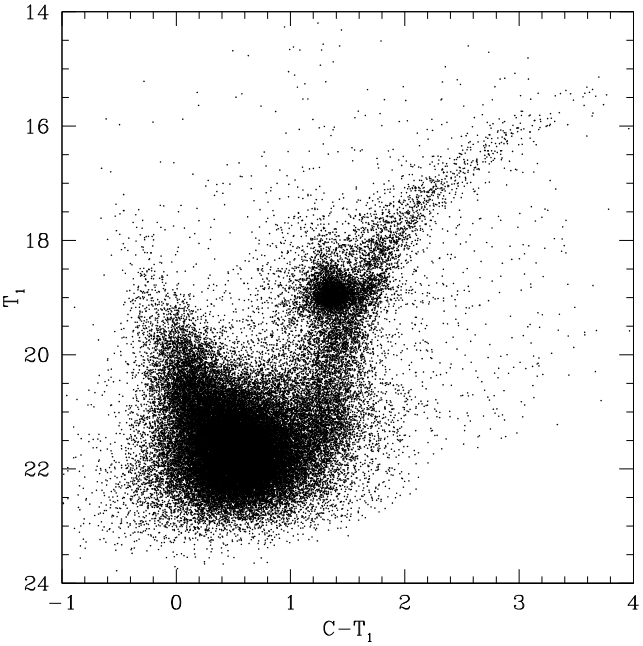

Figure 1. $(C-T_1, T_1)$ CMD for all the measured stars in the field of L28.

Since all the CMDs reveal both cluster and field star features more or less superimposed we should first separate the cluster stars from those belonging to the surrounding fields in order to estimate the cluster fundamental parameters from their CMDs. Note that both cluster and field stars – supposed to be at the same distance – are affected by nearly the same Galactic+SMC reddening, which is indeed what causes the overlapping of their MSs. This fact makes the cleaning process of the CMDs even harder.

To filter the field stars from the CMDs, we essentially applied the frequently used statistical precepts (Hesser et al. 1987; Gratton & Ortolani 1988, among others). We delimited the reference field area to the easternmost strip of the observed fields, i.e. $x < 500$ pixels and $0 < y$ (pixels) < 2050. Note that the clusters are centred on each image and expand over areas smaller than $\sim$100 pixels in radius. From the field CMDs, we statistically clean the cluster CMDs by using bin sizes of $[\Delta T_1, \Delta(C-T_1)] = (0.5, 0.2)$ mag. With the aim of comparing the resulting residuals, we carried out this filtering procedure by using bins of (1.0, 0.2) and (0.5, 0.1) mag. The application of this method rendered 14 additional tables similar to Tables 2–15, one per observed cluster field. Each of them contains the stars that have not been subtracted located within the region delimited by $x > 500$ pixels and $0 < y$ (pixels) < 2050, since we eliminated those matching the spatial density, magnitude and colour distributions of the easternmost strip of the observed fields.

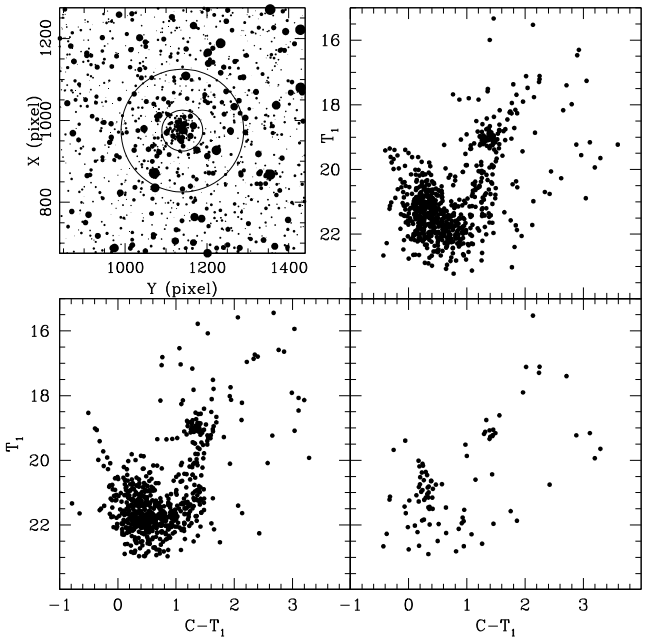

Figure 2. Close-up schematic finding chart of the stars observed in the field of L3 (upper left). North is up and east is to the left. The size of the plotting symbol is proportional to the T_1 brightness of the star. Three extracted CMDs for stars distributed within the close-up region (upper right), the cluster surrounding field for an equal close-up cluster area (bottom left) and the cluster cleaned from field contamination (bottom right) are also depicted (see text for details).

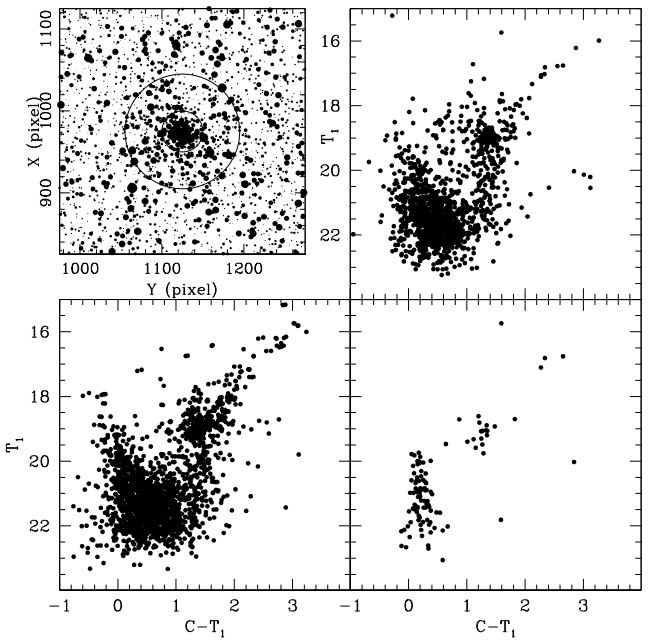

Figure 3. Close-up schematic finding chart of the stars observed in the field of L28 (upper left). North is up and east is to the left. The size of the plotting symbol is proportional to the T_1 brightness of the star. Three extracted CMDs for stars distributed within the close-up region (upper right), the cluster surrounding field for an equal close-up cluster area (bottom left) and the cluster cleaned from field contamination (bottom right) are also depicted (see text for details).

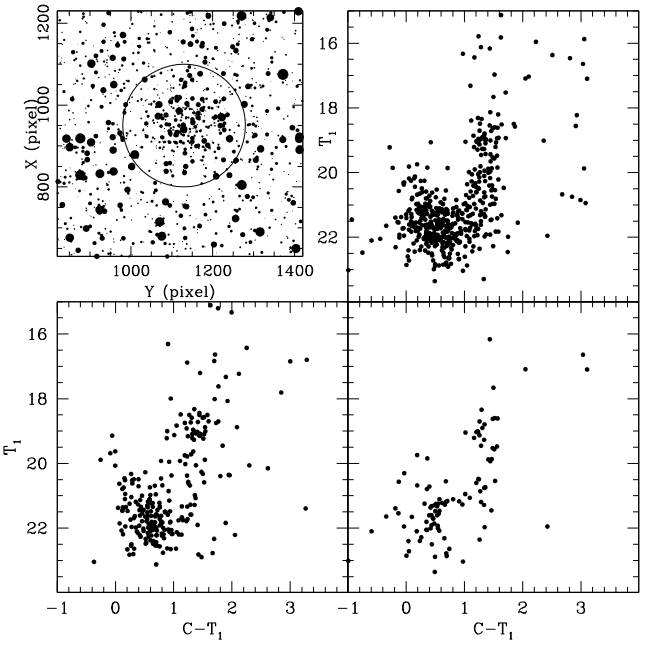

Figure 4. Close-up schematic finding chart of the stars observed in the field of HW 66 (upper left). North is up and east is to the left. The size of the plotting symbol is proportional to the T_1 brightness of the star. Three extracted CMDs for stars distributed within the close-up region (upper right), the cluster surrounding field for an equal close-up cluster area (bottom left) and the cluster cleaned from field contamination (bottom right) are also depicted (see text for details).

Since all the observed clusters are very small in angular extent, we started by estimating the clusters' geometrical centres to obtain circular extracted CMDs where the fiducial features of the clusters could be clearly seen. The cluster centres were estimated by eye using the schematic cluster finding charts which resulted from the above field star cleaned tables. They were finally determined with a typical error of ± 10 pixels ($\sim$4 arcsec). Then, we performed circular extractions and produced different CMDs for each cluster by increasing the radius from its respective centre. Using an equal area field CMD as reference, we chose those radii where the unavoidable residual field contamination becomes significant. We finally adopted both an inner and an outer radius for most of the clusters. The inner radius allowed us to avoid stars closer to the centres whose measures are less accurate owing to their crowding. The outer radius, in turn, can be considered a measure of the cluster extent. This approach enabled us not only to adopt optimum cluster radii but also to obtain CMDs which are representative of the star clusters. Some field star contamination is unavoidable, though.

Figs 2–15 show (top left-hand panels) close-up schematic finding charts of L3, L28, HW 66, L100, HW 79, IC 1708, L106, L108, L109, NGC 643, L112, HW 84, HW 85 and HW 86, respectively. They were drawn using all the measured stars in the different fields. The sizes of the plotting symbols are proportional to the T_1 brightness of the stars. The circles centred on the clusters correspond to the radii used to extract the cluster CMDs. In the top right-hand panels, we depict the CMDs for stars distributed within the top left-hand panels, while the bottom right-hand panels present the cleaned cluster CMDs with stars distributed within their respective adopted circles. The equal close-up cluster area field CMDs are shown in the bottom left-hand panels.

When comparing field and cleaned cluster CMDs, the differences in stellar content become noticeable, as can be seen from the bottom

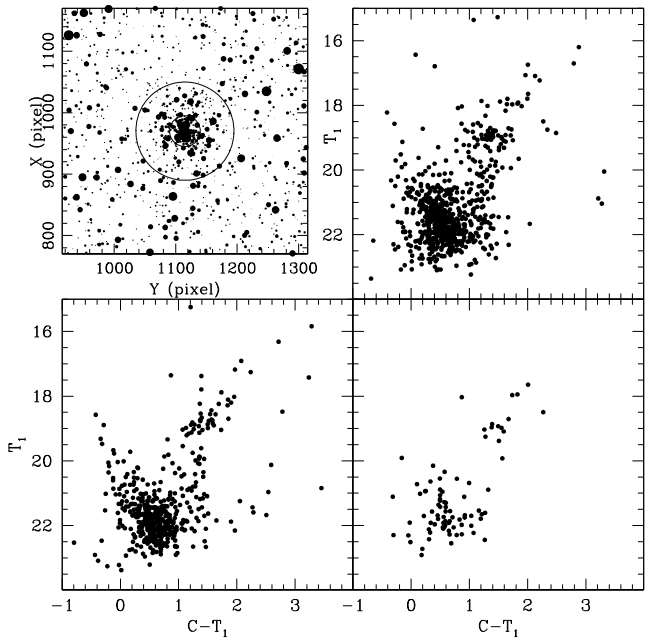

Figure 5. Close-up schematic finding chart of the stars observed in the field of L100 (upper left). North is up and east is to the left. The size of the plotting symbol is proportional to the T_1 brightness of the star. Three extracted CMDs for stars distributed within the close-up region (upper right), the cluster surrounding field for an equal close-up cluster area (bottom left) and the cluster cleaned from field contamination (bottom right) are also depicted (see text for details).

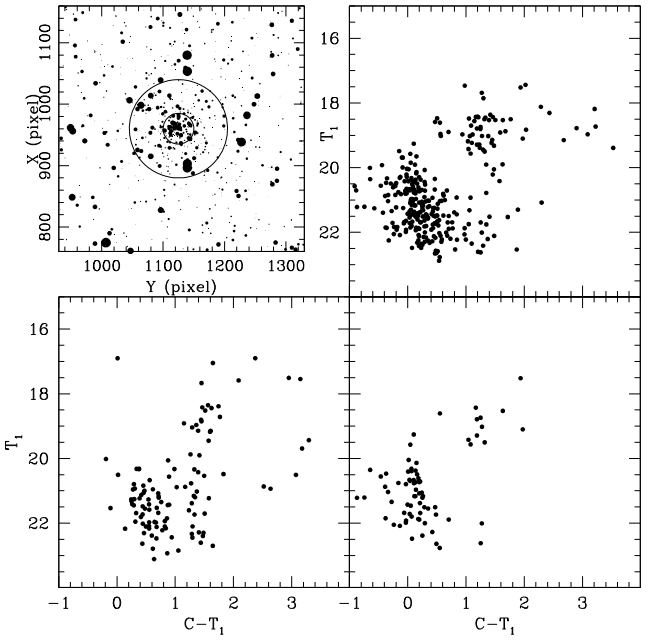

Figure 7. Close-up schematic finding chart of the stars observed in the field of IC 1708 (upper left). North is up and east is to the left. The size of the plotting symbol is proportional to the T_1 brightness of the star. Three extracted CMDs for stars distributed within the close-up region (upper right), the cluster surrounding field for an equal close-up cluster area (bottom left) and the cluster cleaned from field contamination (bottom right) are also depicted (see text for details).

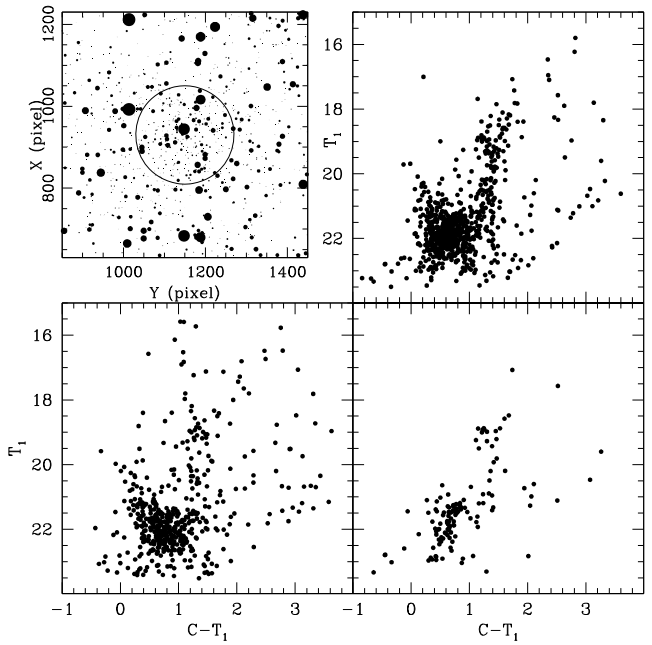

Figure 6. Close-up schematic finding chart of the stars observed in the field of HW 79 (upper left). North is up and east is to the left. The size of the plotting symbol is proportional to the T_1 brightness of the star. Three extracted CMDs for stars distributed within the close-up region (upper right), the cluster surrounding field for an equal close-up cluster area (bottom left) and the cluster cleaned from field contamination (bottom right) are also depicted (see text for details).

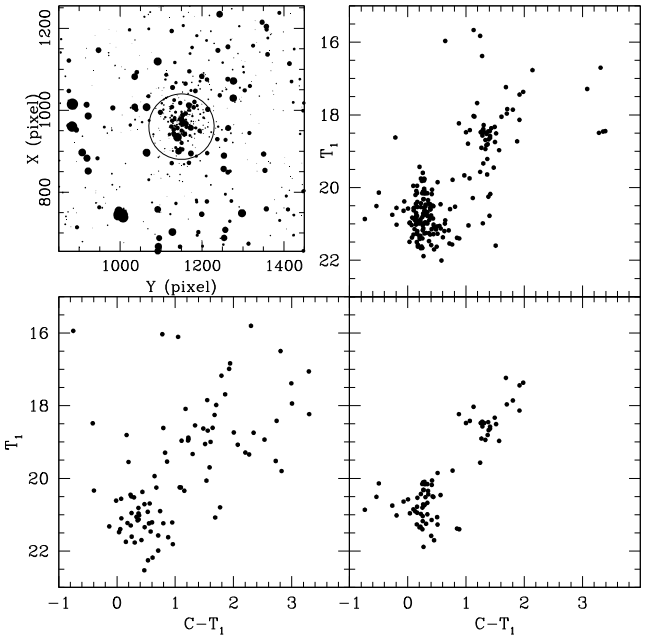

Figure 8. Close-up schematic finding chart of the stars observed in the field of L106 (upper left). North is up and east is to the left. The size of the plotting symbol is proportional to the T_1 brightness of the star. Three extracted CMDs for stars distributed within the close-up region (upper right), the cluster surrounding field for an equal close-up cluster area (bottom left) and the cluster cleaned from field contamination (bottom right) are also depicted (see text for details).

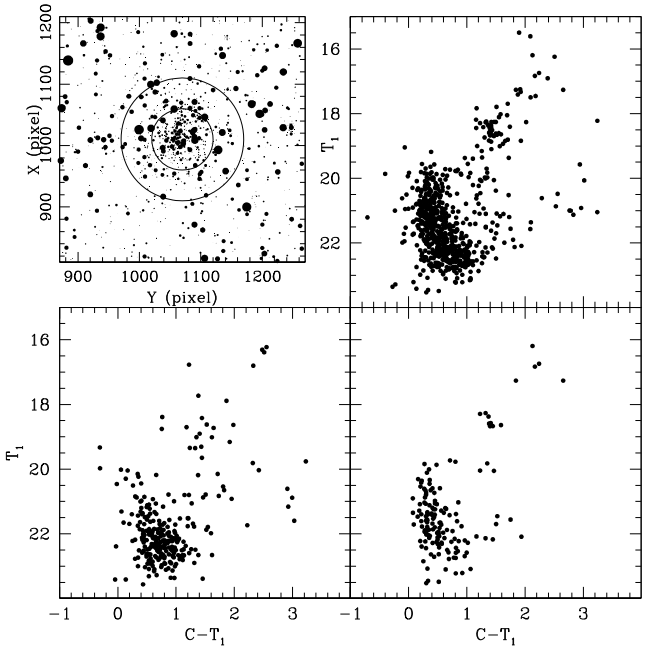

Figure 9. Close-up schematic finding chart of the stars observed in the field of L108 (upper left). North is up and east is to the left. The size of the plotting symbol is proportional to the T_1 brightness of the star. Three extracted CMDs for stars distributed within the close-up region (upper right), the cluster surrounding field for an equal close-up cluster area (bottom left) and the cluster cleaned from field contamination (bottom right) are also depicted (see text for details).

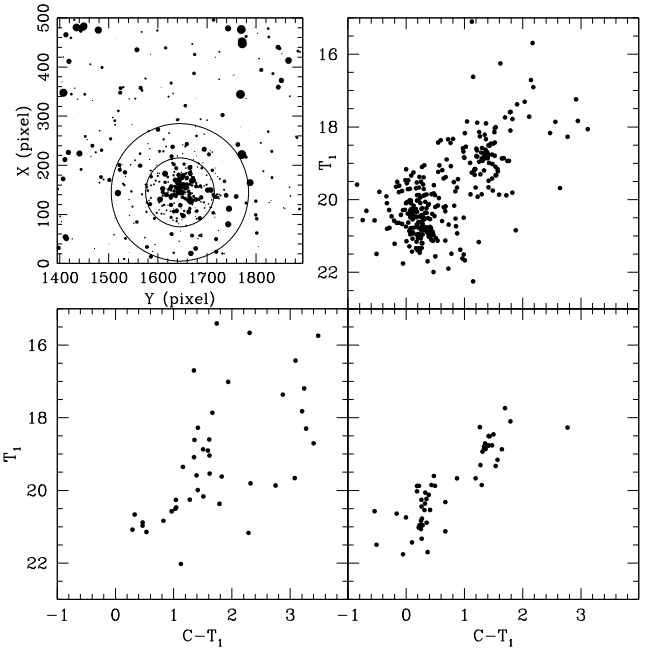

Figure 11. Close-up schematic finding chart of the stars observed in the field of NGC 643 (upper left). North is up and east is to the left. The size of the plotting symbol is proportional to the T_1 brightness of the star. Three extracted CMDs for stars distributed within the close-up region (upper right), the cluster surrounding field for an equal close-up cluster area (bottom left) and the cluster cleaned from field contamination (bottom right) are also depicted (see text for details).

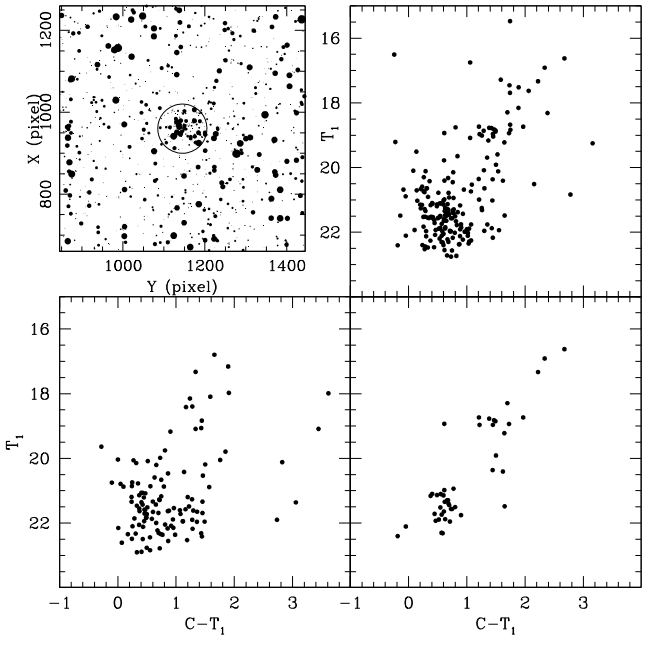

Figure 10. Close-up schematic finding chart of the stars observed in the field of L109 (upper left). North is up and east is to the left. The size of the plotting symbol is proportional to the T_1 brightness of the star. Three extracted CMDs for stars distributed within the close-up region (upper right), the cluster surrounding field for an equal close-up cluster area (bottom left) and the cluster cleaned from field contamination (bottom right) are also depicted (see text for details).

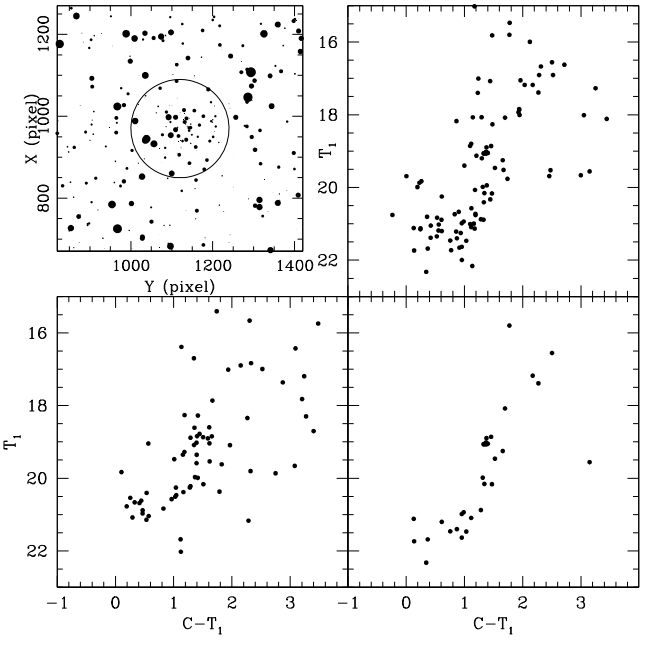

Figure 12. Close-up schematic finding chart of the stars observed in the field of L112 (upper left). North is up and east is to the left. The size of the plotting symbol is proportional to the T_1 brightness of the star. Three extracted CMDs for stars distributed within the close-up region (upper right), the cluster surrounding field for an equal close-up cluster area (bottom left) and the cluster cleaned from field contamination (bottom right) are also depicted (see text for details).

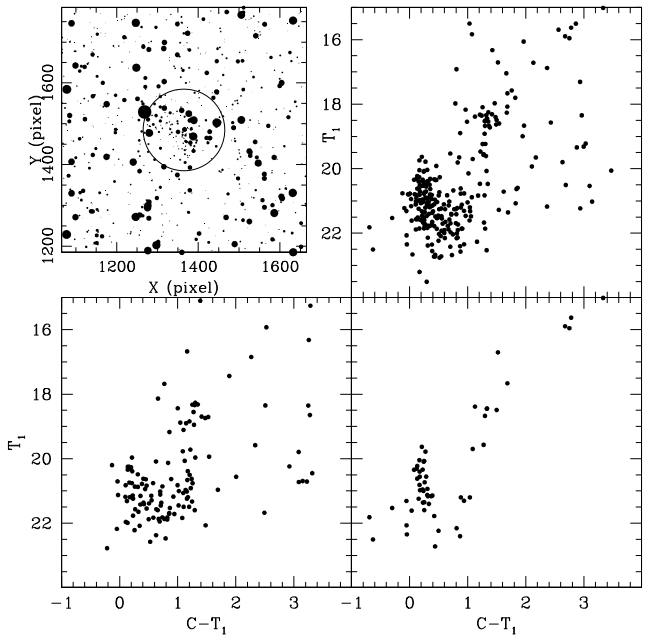

Figure 13. Close-up schematic finding chart of the stars observed in the field of HW 84 (upper left). North is up and east is to the left. The size of the plotting symbol is proportional to the T_1 brightness of the star. Three extracted CMDs for stars distributed within the close-up region (upper right), the cluster surrounding field for an equal close-up cluster area (bottom left) and the cluster cleaned from field contamination (bottom right) are also depicted (see text for details).

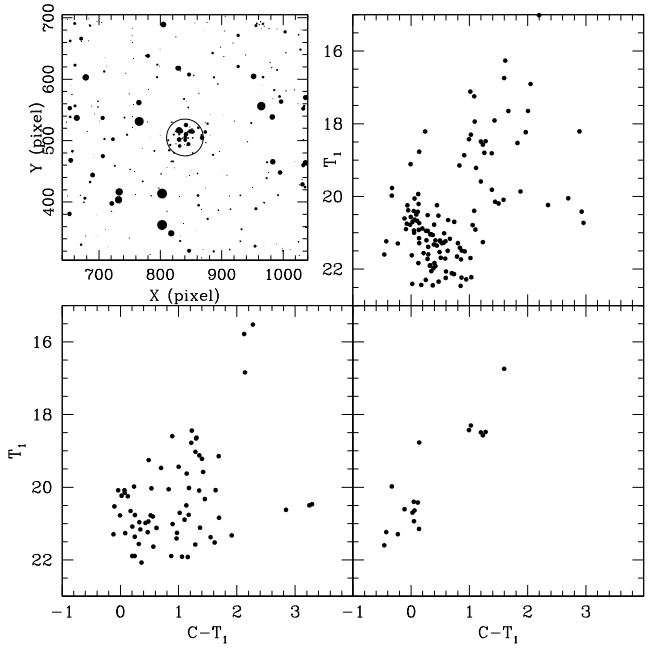

Figure 14. Close-up schematic finding chart of the stars observed in the field of HW 85 (upper left). North is up and east is to the left. The size of the plotting symbol is proportional to the T_1 brightness of the star. Three extracted CMDs for stars distributed within the close-up region (upper right), the cluster surrounding field for an equal close-up cluster area (bottom left) and the cluster cleaned from field contamination (bottom right) are also depicted (see text for details).

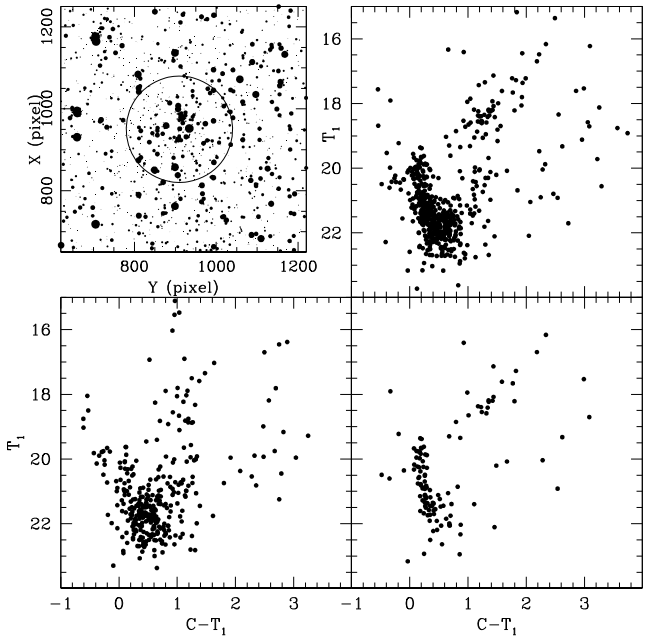

Figure 15. Close-up schematic finding chart of the stars observed in the field of HW 86 (upper left). North is up and east is to the left. The size of the plotting symbol is proportional to the T_1 brightness of the star. Three extracted CMDs for stars distributed within the close-up region (upper right), the cluster surrounding field for an equal close-up cluster area (bottom left) and the cluster cleaned from field contamination (bottom right) are also depicted (see text for details).

panels of Figs 2–15. Particularly, the field RC at $T_1 \sim 19$ (which becomes prominent for age ∼1–5 Gyr) is the most common field feature, in addition to the field MS composed of stars within a probable wide age range. The CMDs of L3, L28, L100, IC 1708, L106, L108, L109, NGC 643, HW 84 and HW 86 – which exhibit clear RCs – resemble those of intermediate-age star clusters around 1 Gyr old, whereas the CMDs of HW 66, HW 79 and L112 – which show RGBs – seem to correspond to older clusters. In fact, Piatti et al. (2007b) found an age of 5.3 Gyr for L112.

4 ESTIMATES OF THE CLUSTERS' FUNDAMENTAL PARAMETERS

The estimation of cluster reddening values was made by interpolating the extinction maps of Burstein & Heiles (1982, hereafter BH). BH maps were obtained from H I (21 cm) emission data for the southern sky. They furnish us with foreground $E(B-V)$ colour excesses which depend on the Galactic coordinates. Schlegel, Finkbeiner & Davis (1998, hereafter SFD) obtained full-sky maps from 100-μm dust emission. They found that, at high latitudes, the dust map correlates well with maps of H I emission. However, deviations are coherent in the sky and are especially conspicuous in regions of saturation of H I emission towards denser clouds and of formation of H_2 in molecular clouds (Piatti et al. 2003b, 2008). We used SFD's reddening maps to prove that when maximum and minimum extinction values are compared, the interstellar reddening is uniform across the observed fields, which may not happen in certain regions of the sky. We computed $E(B-V)_{\rm SFD}$ colour excesses for grids in the (l, b) Galactic coordinate plane, with steps of $\Delta(l,\, b) = (0.^{\circ}01,\, 0.^{\circ}01)$ covering the whole observed fields. We obtained between 80 and 100 colour excess values per cluster field. Then, for the resulting $E(B-V)_{\rm SFD}$ values, we built histograms and

Table 18. Fundamental parameters of SMC clusters.

Name	$E(B-V)$ (mag)				Age (Gyr)		[Fe/H]	
	BH	SFD (min)	SFD (max)	Adopted	Isochrone	δT_1	Isochrone	SGB
L3	0.03	0.04	0.04	0.04	1.00 ± 0.25	1.25 ± 0.20	-0.7	-0.65 ± 0.2
L28	0.06	0.07	0.09	0.08	0.80 ± 0.20	1.20 ± 0.30	-0.7	-0.75 ± 0.2
HW 66	0.04	0.05	0.05	0.05	4.00 ± 0.90	3.50 ± 1.00	-1.3	-1.35 ± 0.2
L100	0.03	0.04	0.05	0.04	2.00 ± 0.50	2.30 ± 0.60	-0.7	–
HW 79	0.05	0.06	0.07	0.06	5.00 ± 1.30	4.30 ± 1.20	-1.3	-1.4 ± 0.2
IC 1708	0.03	0.04	0.04	0.04	0.60 ± 0.20	–	-0.7	–
L106	0.05	0.05	0.05	0.05	1.10 ± 0.25	2.00 ± 0.90	-0.7	–
L108	0.03	0.04	0.04	0.04	1.10 ± 0.25	1.60 ± 0.30	-0.7	–
L109	0.04	0.04	0.05	0.04	2.50 ± 0.60	3.50 ± 1.00	-0.7	-1.0 ± 0.2
NGC 643	0.05	0.07	0.07	0.07	1.00 ± 0.25	1.40 ± 0.20	-0.7	-0.7 ± 0.2
L112	0.05	0.07	0.07	0.07	6.30 ± 1.40	$\gtrapprox 5.00$	-1.3	-1.4 ± 0.2
HW 84	0.02	0.03	0.03	0.03	0.90 ± 0.20	1.40 ± 0.20	-0.7	–
HW 85	0.02	0.03	0.03	0.03	1.10 ± 0.25	2.20 ± 0.50	-1.3	–
HW 86	0.03	0.04	0.04	0.04	0.80 ± 0.20	1.40 ± 0.20	-0.7	–

calculated their centres and full width at half-maximum (FWHM) values. Since the FWHM values turned out to be quite small, we assumed that the interstellar absorption is uniform across each cluster field. Table 18 lists the $E(B-V)_{\rm BH}$ colour excesses, the minimum and maximum values of $E(B-V)_{\rm SFD}$ and the adopted cluster reddenings. The $A_{T_1}/E(B-V)$ and $E(C-T_1)/E(B-V)$ ratios given by Geisler & Sarajedini (1999) were then used to enter the CMDs with the corresponding M_{T_1} and $(C-T_1)_0$ values.

As for the cluster distance moduli, we adopted for all of them the value of the SMC distance modulus $(m-M)_0 = 18.90 \pm 0.10$ recently reported by Glatt, Grebel & Koch (2010). Considering BH reddening values for populous SMC clusters, Crowl et al. (2001) found the line-of-sight depth of the galaxy to be approximately 6 kpc. Then, bearing in mind that any cluster of the sample could be placed in front of or behind the main body of the SMC, we concluded that the difference in apparent distance modulus could be as large as $\Delta(V-M_V) \sim 0.2$ mag, if a value of 60 kpc is adopted for the mean SMC distance. Given the fact that an uncertainty of 0.2–0.3 mag was estimated when adjusting the isochrones to the cluster CMDs in magnitude, our simple assumption of adopting a unique value for the distance modulus for all the clusters should not dominate the error budget in our final results. In fact, when overplotting the zero-age main sequence (ZAMS) on the observed cluster CMDs, previously shifted by the $E(B-V)$ of Table 18 and $(m-M)_0 = 18.90$, an excellent match was generally found.

In order to estimate the cluster ages, it must be taken into account that cluster metallicity plays an important role when fitting theoretical isochrones. The distinction is mainly evident for the evolved RC and RGB phases. ZAMSs are often less affected by metallicity effects and can even exhibit imperceptible variations for a specific metallicity range within the expected photometric errors. We took advantage of the available theoretical isochrones computed for the Washington photometric system to estimate cluster ages. We used the isochrones calculated with core overshooting included by the Padova group (Girardi et al. 2002). These isochrones led to results similar to those derived if the Geneva group's (Lejeune & Schaerer 2001) had been used. Nevertheless, the former reach fainter luminosities which allows a better fit to the fainter portions of the MS.

When we chose subsets of isochrones for different Z metallicity values to evaluate the metallicity effect in the cluster fundamental parameters, we preferred to follow the general rule of starting without assuming any pre-arranged metallicity. Instead, we adopted chemical compositions of $Z = 0.001$, 0.004 and 0.008 ([FeH] = -1.3, -0.7 and -0.4, respectively) for the isochrone sets which cover the metallicity range of most of the SMC clusters studied in detail so far (Parisi et al. 2009). We then selected a set of isochrones, along with the equations $E(C-T_1) = 1.97E(B-V)$ and $M_{T_1} = T_1 + 0.58E(B-V) - (V-M_V)$ (Geisler & Sarajedini 1999), and superimposed them on the cluster CMDs, once they were properly shifted by the corresponding $E(B-V)$ colour excesses and by the SMC apparent distance modulus. In the matching procedure, we used seven different isochrones for each metallicity level, ranging from slightly younger than the derived cluster age to slightly older. Finally, we adopted as the cluster age the one corresponding to the isochrone which best reproduced the cluster main features in the CMD. The presence of RCs and/or RGBs in some cluster CMDs made the fitting procedure easier. We noted, however, that the theoretically computed bluest stage during the He-burning core phase is redder than the observed RC in the CMDs of some clusters, a behaviour already detected in other studies of Galactic and Magellanic Cloud clusters (e.g. Geisler et al. 2003; Piatti, Clariá & Ahumada 2004a,b). A similar outcome was found from the fitting of isochrones in the M_V versus $(V-I)_{\rm o}$ diagram (Piatti, Clariá & Ahumada 2003a,d, among others). Figs 16–19 show the results of the fittings. For each cluster CMD, we plotted the isochrone of the adopted cluster age (solid lines) and two additional isochrones bracketing the derived age (dotted lines). The ages of the bracketing isochrones were estimated by taking into account the observed dispersion in the cluster CMDs. The ages of the adopted isochrones and their corresponding metallicities for the cluster sample are listed in Table 18.

We also derived cluster ages from the δT_1 index, calculated by determining the difference in the T_1 magnitude of the RC and the MS TO in the cluster CMDs. An uncertainty of $\langle \sigma_{\rm TO} \rangle = 0.20$ mag was assigned to the TO T_1 magnitude. In view of the crowded nature of some cluster fields, of the rather sparse RC and especially of the somewhat subjective nature of this procedure, slightly larger errors may appear. We then derived the cluster ages from the corresponding δT_1 values using equation (4) of Geisler et al. (1997). The resulting values are listed in column 7 of Table 18. It can be seen that they are in very good agreement with those derived from the isochrone fittings, which confirms that both methods allowed us to estimate ages in a similar scale. So it was not necessary to apply any zero-point offset. On the other hand, our resulting ages for L108 and L112 (see also Table 18) show an excellent agreement with those

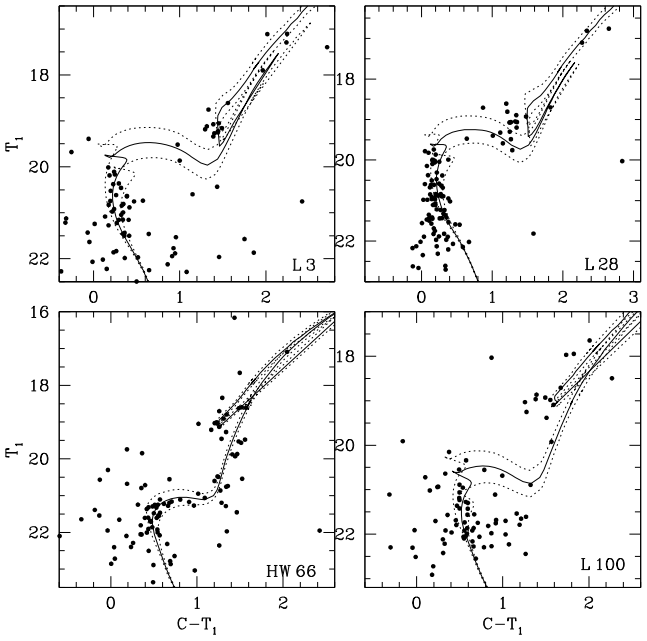

Figure 16. Cleaned Washington T_1 versus $C - T_1$ CMDs for the selected star clusters. Isochrones from Girardi et al. (2002), computed taking into account overshooting, are overplotted. The solid and dashed lines correspond to the derived clusters' age and to the ages obtained taking into account their associated errors (see columns 6 and 8 of Table 19), respectively: $\log(t) = 8.90$, 9.00 and 9.10 and $Z = 0.004$ for L3 (upper left); $\log(t) = 8.80$, 8.90 and 9.00 and $Z = 0.004$ for L28 (upper right); $\log(t) = 9.50$, 9.60 and 9.70 and $Z = 0.001$ for HW 66 (bottom left); $\log(t) = 9.20$, 9.30 and 9.40 and $Z = 0.004$ for L100 (bottom right).

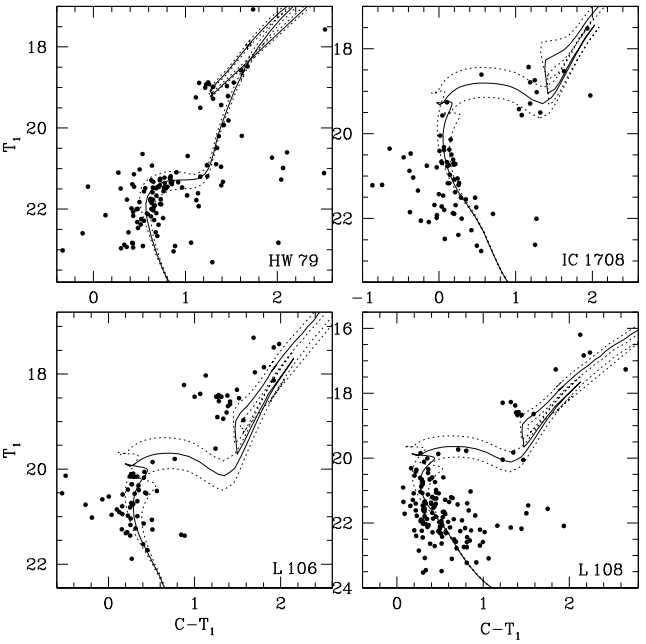

Figure 17. Cleaned Washington T_1 versus $C - T_1$ CMDs for the selected star clusters. Isochrones from Girardi et al. (2002), computed taking into account overshooting, are overplotted. The solid and dashed lines correspond to the derived clusters' age and to the ages obtained taking into account their associated errors (see columns 6 and 8 of Table 19), respectively: $\log(t) = 9.60$, 9.70 and 9.80 and $Z = 0.001$ for HW 79 (upper left); $\log(t) = 8.70$, 8.80 and 8.90 and $Z = 0.004$ for IC 1708 (upper right); $\log(t) = 8.95$, 9.05 and 9.15 and $Z = 0.004$ for L106 (bottom left); $\log(t) = 8.95$, 9.05 and 9.15 and $Z = 0.004$ for L108 (bottom right).

derived by Piatti et al. (2007b,c). We then reproduced the cluster age scale of Piatti et al. (2008) which will be used in the subsequent analysis on the formation history of clusters in the SMC.

We then followed the standard giant branch (SGB) procedure of entering into fig. 4 of Geisler & Sarajedini (1999) absolute M_{T_1} magnitudes and intrinsic $(C - T_1)_0$ colours to roughly derive the cluster metal abundances [Fe/H] by interpolation (Figs 16–19). The metallicities herein derived were then corrected for age effects following the prescriptions given in Geisler et al. (2003). Metallicities could be estimated only for some of the clusters, provided their CMDs showed more or less visible SGB stars. The final age-corrected [Fe/H] values are listed in column 9 of Table 18. There is a remarkable agreement between these values and those corresponding to the isochrones which best resemble the cluster CMDs (column 8 of Table 18). Note that Piatti et al. (2007b) estimated [Fe/H] $= -1.1 \pm 0.25$ for L112, which is – within the quoted uncertainties – comparable to the present value. Parisi et al. (2009) also derived from Ca II triplet lines [Fe/H] values of -1.05 ± 0.05 and -0.82 ± 0.03 for L108 and NGC 643, respectively. Although the [Fe/H] value for L108 is somewhat different from that associated with the cluster isochrone age, a very good agreement was found for NGC 643. Note that Girardi et al. (2002) models are computed for [Fe/H] $= -1.3$ and -0.7 dex but not for in-between metallicity values.

5 ANALYSIS AND DISCUSSION

Recent studies have appeared in the literature with a view to improving our knowledge about the SMC age–metallicity relation (AMR; Piatti et al. 2007b; Parisi et al. 2009), about its hierarchical structure (Bonatto & Bica 2010), about the age distribution of young clusters and the recent SMC star formation (Chiosi et al. 2006; Glatt et al. 2010) and about the cluster infant mortality phenomenon and disruption rate (de Grijs & Goodwin 2008; Chandar, Fall & Whitmore 2010). From a theoretical point of view, Tsujimoto & Bekki (2010) have just reported evidence that a major merger is imprinted in the AMR as a dip in [Fe/H], which occurred ∼7.5 Gyr ago. However, as far as we know, no thorough age distribution study has lately been performed for the SMC clusters older than 1.0 Gyr. This section is devoted to dealing with this issue.

We first searched in the literature for previous SMC studies on cluster age determinations. Using an age scale where L1 is 9 Gyr, Mighell, Sarajedini & French (1998, hereafter MSF) estimated the ages of seven old SMC clusters. They included in their analysis the ages of five young SMC clusters discussed in Da Costa & Hatzidimitriou (1998), which represent the present day properties of the SMC. In recent years, we have developed a long-term programme to estimate the ages of unstudied or poorly studied SMC clusters, based on measurements in the Washington photometric system. These age and metallicity measures rely primarily on the age-calibrated δT_1 index. As pointed out by Piatti et al. (2001, 2007b), the ages estimated with this technique are in the age scale of MSF. Besides, once their metallicities were fixed, we fitted theoretical isochrones to the cluster (T_1, $C - T_1$) CMDs in order to estimate their ages. We showed that the derived values are in very good agreement with those obtained from δT_1 for clusters for which we applied both techniques (Piatti et al. 2002; Geisler et al. 2003). Hence, we can also assume that these clusters are on the same age scale as MSF. We also included additional clusters with ages derived from integrated spectra (Piatti et al. 2005a) to enlarge our cluster sample. Piatti et al. (2005a) observed a total of 18 clusters and

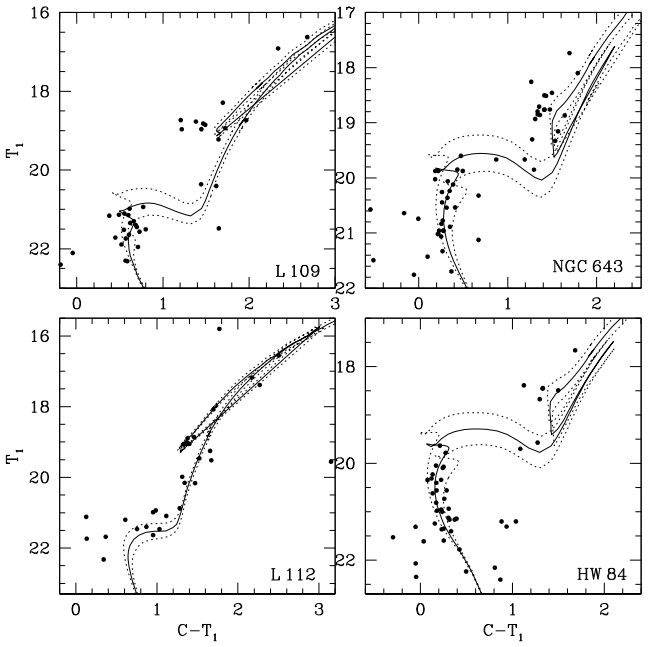

Figure 18. Cleaned Washington T_1 versus $C - T_1$ CMDs for the selected star clusters. Isochrones from Girardi et al. (2002), computed taking into account overshooting, are overplotted. The solid and dashed lines correspond to the derived clusters' age and to the ages obtained taking into account their associated errors (see columns 6 and 8 of Table 19), respectively: $\log(t) = 9.30$, 9.40 and 9.50 and $Z = 0.004$ for L109 (upper left); $\log(t) = 8.90$, 9.00 and 9.10 and $Z = 0.004$ for L111 (upper right); $\log(t) = 9.70$, 9.80 and 9.90 and $Z = 0.001$ for L112 (bottom left); $\log(t) = 8.85$, 8.95 and 9.05 and $Z = 0.004$ for HW 84 (bottom right).

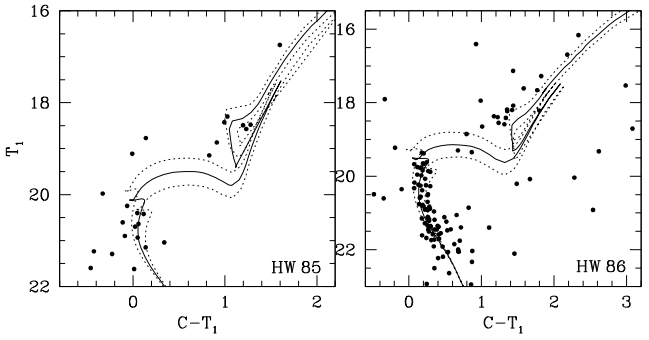

Figure 19. Cleaned Washington T_1 versus $C - T_1$ CMDs for the selected star clusters. Isochrones from Girardi et al. (2002), computed taking into account overshooting, are overplotted. The solid and dashed lines correspond to the derived clusters' age and to the ages obtained taking into account their associated errors (see columns 6 and 8 of Table 19), respectively: $\log(t) = 8.95$, 9.05 and 9.15 and $Z = 0.001$ for HW 85 (left); $\log(t) = 8.80$, 8.90 and 9.00 and $Z = 0.004$ for HW 86 (right).

found that the ages of nine of them, derived from previous studies in the MSF scale, are in good agreement with their own estimates. Finally, we included three clusters (AM 3, BS 90 and BS 196) with ages estimated from theoretical isochrones fittings on to the cluster CMDs, which we assume to be equivalent to our Washington CMDs fittings. Table 19 presents all the collected clusters with reliable age estimates, along with their age uncertainties and references. We now have available a total sample of 43 well known clusters older than 1 Gyr, including the 14 clusters of the present study.

The histogram of the cluster ages is frequently built using a fixed age bin of ∼100–500 Myr. This age bin makes it difficult to distinguish any intrinsic fluctuations along the younger range, while the older clusters turn out to be almost subsampled. Piatti (2010) showed that a fixed age bin size is not appropriate to obtain an intrinsic age distribution since the histogram result depends on the chosen age interval. A more suitable age interval should be the one whose width is a measure of the cluster age errors in that interval. This would lead to the choice of very narrow bins for younger clusters and relatively broader age bins for older ones.

To build an age histogram that tightly reproduces the intrinsic clusters' age distribution, we considered the uncertainties in the age estimates to define the age intervals in the whole cluster age range of Table 19. In this way, we got a more appropriate sampling of the clusters per age interval than if we had used a fixed bin size, since we included in each bin a number of clusters whose age errors were close to the size of this bin. In fact, the age errors for young clusters are in general a few Myr, while those for older clusters are at least a few Gyr. Therefore, smaller bins are appropriate for younger clusters, whereas larger bins are suitable for older ones. We then searched Table 19 and found that typical age errors lie in the $0.05 \lesssim \Delta\log(t) \lesssim 0.10$ interval. Therefore, we produced a new age histogram by setting the bin sizes according to this logarithmic law, which traces the variation in the derived age uncertainties in terms of the cluster ages. We used intervals of $\Delta\log(t) = 0.20$, since if we had used $\Delta\log(t) = 0.10$, we would have obtained a slightly noisier histogram. Thus, the subdivision of the whole age range in age intervals of different sizes can be performed on an observational-based foundation, as they are a measure of the typical cluster age errors for each age range.

Apart from the variation of the age bin sizes in terms of the estimated age errors, there is another source of uncertainty in the number of clusters per age bin that depends on the age used to define the lower limit of the age histogram. For this reason, we produced four different cluster age histograms with successive starting points at $\log(t) = 8.90$, 8.95, 9.00 and 9.05, respectively. Fig. 20 displays the resulting averaged age histogram with the error bars included. Notice that, although the four histograms were calculated using bins of $\Delta\log(t) = 0.10$, Fig. 20 was resampled into 1 Gyr wide bins.

Fig. 20 shows that the SMC cluster system seems, at first glance, to have experienced two enhanced formation processes that peaked at $t \sim 2$ and 5 Gyr, the former being more prominent and constrained in time. Note that we focused on clusters older than 1 Gyr for which we used the most complete and homogeneous sample known up to now. Moreover, tracing the variation of the histogram slope from older to younger ages, we found that from the birth of the SMC cluster system until approximately the first 4 Gyr of its lifetime, the cluster formation resembles that of a constant formation rate scenario. In fact, the slope of the cluster age distribution does not change in the ∼8–12 Gyr age range. Note that the assumption of a constant disruption rate would not alter such a trend. A simple closed system with continuous star formation under the assumption of a chemical homogeneity as modelled by Da Costa & Hatzidimitriou (1998) could correspond to this period. Later on, at $t \sim$ 7–8 Gyr, the age distribution presents an abrupt change in the slope as a consequence of a sudden appearance of a relative excess of clusters. Such an excess could arise from an enhanced cluster formation event triggered by the tidal interaction between both MCs. Indeed, Tsujimoto & Bekki (2010) suggested that the predicted merger event at $t \sim 7.5$ Gyr took place in a small group environment that was far from the Galaxy and contained a number of small gas-rich dwarfs comparable to the SMC. However, although this theoretical view is

Table 19. Ages of SMC clusters.

Name	Age (Gyr)	Source[a]	Name	Age (Gyr)	Source[a]
AM 3	5.5 ± 1.50	9	L17	1.26 ± 0.20	12
B34	1.20 ± 0.30	5	L19	2.10 ± 0.30	4
BS 90	4.50 ± 0.10	10	L27	2.10 ± 0.30	4
BS 121	2.30 ± 0.40	4	L28	1.00 ± 0.30	13
BS 196	5.00 ± 0.50	11	L32	4.80 ± 0.50	3
HW 47	2.80 ± 0.50	4	L38	6.00 ± 0.60	3
HW 66	3.80 ± 1.00	13	L100	2.10 ± 0.60	13
HW 79	4.70 ± 1.30	13	L106	1.60 ± 0.60	13
HW 84	1.20 ± 0.40	13	L108	1.40 ± 0.30	13
HW 85	1.80 ± 0.50	13	L109	3.00 ± 0.80	13
HW 86	1.10 ± 0.30	13	L110	6.40 ± 0.90	6
K3	9.00 ± 2.00	2	L112	6.50 ± 0.90	6, 13
K6	1.60 ± 0.40	8	L113	6.00 ± 1.00	2, 6
K7	3.50 ± 1.00	2, 3	NGC 121	12.00 ± 2.00	2
K28	2.10 ± 0.60	3	NGC 152	1.90 ± 0.50	2
K44	3.10 ± 0.80	3	NGC 339	4.00 ± 1.50	2
L1	10.00 ± 1.00	2	NGC 361	8.10 ± 1.20	1
L3	1.15 ± 0.25	13	NGC 411	1.50 ± 0.30	2
L4	3.10 ± 0.60	4	NGC 416	6.90 ± 1.10	1
L5	4.10 ± 1.50	4	NGC 419	1.20 ± 0.15	2
L6	3.30 ± 0.70	4	NGC 643	1.10 ± 0.20	7, 13
L7	2.00 ± 0.50	4			

[a]1 – Mighell et al. (1998); 2 – Da Costa & Hatzidimitriou (1998); 3 – Piatti et al. (2001); 4 – Piatti et al. (2005b); 5 – Piatti et al. (2007c); 6 – Piatti et al. (2007b); 7 – Piatti et al. (2007a); 8 – Piatti et al. (2005a); 9 – Da Costa (1999); 10 – Rochau et al. (2007); 11 – Bica et al. (2008b); 12 – Rafelski & Zaritsky (2005); 13 – present work.

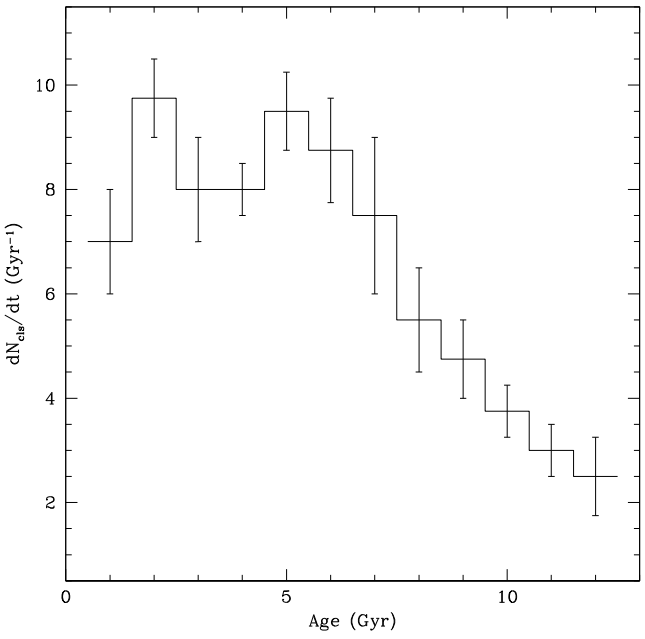

Figure 20. The intrinsic age distribution of SMC clusters listed in Table 5.

extensively discussed by Tsujimoto & Bekki in the framework that considers a connection with the formation history of the LMC, we remark that LMC cluster excesses have not even been detected at this age. Piatti et al. (2002) showed that the cluster AMR of both MCs between 12 and 15 Gyr is only populated by LMC clusters, whereas SMC clusters are found during the LMC age gap. The sole exception in the latter is ESO 121−SC03 (Geisler et al. 1997). Moreover, assuming that the LMC gap is real, i.e. there existed a quiescent period of cluster formation in the LMC and also assuming that the first SMC clusters were formed ∼12 Gyr ago (NGC 121), Piatti et al. (2002) suggested the following possible scenario: the SMC was formed from a tearing of some part of the LMC containing gas and and/or star clusters, possibly due to the interaction between the LMC and our Galaxy.

Fig. 20 also shows that this first enhanced formation process peaked at $t \sim 5$ Gyr, followed by a relatively slower cluster formation period of ∼2 Gyr. Then, at $t \sim 2$ Gyr, a second peak appears, a fact that is generally attributed to a bursting cluster formation episode generated by the interaction between both MCs. The existence of this peak has been widely shown in the literature. For example, the enlarged SMC star cluster sample of Piatti et al. (2007b) (included in Table 19) strengthens the observed AMR, making it more consistent with the bursting star formation history of Pagel & Tautvaišienė (1998) than with the simple closed system with continuous star formation of Da Costa & Hatzidimitriou (1998). Previous studies favouring the bursting star formation scenario in the SMC are those of MSF, Rich et al. (2000), Bekki et al. (2004) and Piatti et al. (2005b), among others. In this sense, although Fig. 20 illustrates the most unfavourable situation – recall that it takes into account the errors of each age estimate – it even proves the existence of such peak within a confidence level higher than 70 per cent.

On the other hand, evidence of triggered episodes of cluster formation within a narrow age range at ∼2 Gyr (Piatti et al. 2002, 2009) has also been found in the LMC. In fact, Piatti et al. (2003c) used a homogenous LMC star cluster sample to show that the cluster excess at ∼2 Gyr is better reproduced by the bursting model of Pagel & Tautvaišienė than by the closed-box enrichment model computed by Geha et al. (1998), using the star formation history of Holtzman

et al. (1997). It is hard to explain that the similar ages of the cluster excess peaks found in both MCs are due to mere coincidence. They are most probably due to the close interaction between them. In such case, the existence of a cluster excess in the SMC at ∼2 Gyr (Chiosi et al. 2006; Piatti et al. 2007b) is largely favoured.

6 SUMMARY AND CONCLUSIONS

As part of a continuing project to investigate the cluster formation and chemical evolution history of the SMC, we have used the CTIO 1.5-m telescope to obtain CCD imaging in the Washington system of 14 SMC star clusters. We present here the CMDs of L3, L28, HW 66, L100, HW 79, IC 1708, L106, L108, L109, NGC 643, L112, HW 84, HW 85 and HW 86. The analysis of their photometric data leads to the following main conclusions.

(i) We applied a subtraction procedure to statistically clean the cluster CMDs from field star contamination in order to disentangle cluster features from those belonging to their surrounding fields. The 14 clusters turned out to be relatively small angular sized objects.

(ii) Using the cleaned cluster (T_1, $C - T_1$) diagrams, we estimated ages and metallicities from theoretical isochrones computed for the Washington system. We also estimated ages from the $\delta(T_1)$ index and metallicities by applying the SGB procedure. With the exception of IC 1708, a relatively metal-poor Hyades-age cluster, the remaining 13 objects are between intermediate and old ages, whose [Fe/H] values vary from −1.4 to −0.7 dex.

(iii) By combining these results with others available in the literature, we compiled a sample of 43 well-known clusters older than 1 Gyr. Then, by adopting an age interval varying in terms of age according to a logarithmic law, we built a new cluster age histogram, which proved to trace the intrinsic age distribution more properly. The revised age distribution can be considered to statistically represent the population between intermediate and old ages.

(iv) The obtained cluster age distribution reveals two primary excesses at $t \sim 2$ and 5 Gyr, which are possible signs of enhanced formation episodes, similar to those reported for other galaxies. The peak at ∼2 Gyr seems to be more prominent and constrained in time. In addition, we found that from the birth of the SMC cluster system until approximately the first 4 Gyr of its lifetime, the cluster formation resembles that of a constant formation rate scenario.

ACKNOWLEDGMENTS

We thank the anonymous referee for his/her valuable comments which helped us to improve the manuscript. We are gratefully indebted to the CTIO staff for their hospitality and support during the observing run. This work was partially supported by the Argentinian institutions CONICET and Agencia Nacional de Promoción Científica y Tecnológica (ANPCyT). EB acknowledges support from the Brazilian Institutions CNPq and CAPES.

REFERENCES

Bastian N., Gieles M., Ercolano B., Gutermuth R., 2009, MNRAS, 392, 868
Bekki K., Couch W. J., Beasley M. A., Forbes D. A., Chiba M., Da Costa G. S., 2004, ApJ, 610, L93
Bica E., Schmitt H. R., 1995, ApJS, 101, 41
Bica E., Schmitt H. R., Dutra C. M., Oliveira H. L., 1999, AJ, 117, 238
Bica E., Bonatto C., Dutra C. M., Santos J. F. C., Jr, 2008a, MNRAS, 389, 678
Bica E., Santos J. F. C., Jr, Schmidt A. A., 2008b, MNRAS, 391, 915
Bonatto C., Bica E., 2010, MNRAS, 403, 996
Burstein D., Heiles C., 1982, AJ, 87, 1165 (BH)
Canterna R., 1976, AJ, 81, 228
Chandar R., Fall S. M., Whitmore B. C., 2010, ApJ, 711, 1263
Chiosi E., Vallenari A., Held E. V., Rizzi L., Moretti A., 2006, A&A, 452, 179
Cioni M. R. et al., 2011, A&A, 527, 116
Crowl H. H., Sarajedini A., Piatti A. E., Geisler D., Bica E., Clariá J. J., Santos J. F. C., Jr, 2001, AJ, 122, 220
Da Costa G. S., 1991, in Haynes R., Milne D., eds, Proc. IAU Symp. 148, The Magellanic Clouds. Kluwer, Dordrecht, p. 183
Da Costa G. S., 1999, in Chu Y. H., Suntzeff N., Hesser J., Bohlender D., eds, Proc. IAU Symp. 190, New Views of the Magellanic Clouds. Cambridge Univ. Press, Cambridge, p. 446
Da Costa G. S., Hatzidimitriou D., 1998, AJ, 115, 1934
de Grijs R., Goodwin S. P., 2008, MNRAS, 383, 1000
Gallart C., 1998, ApJ, 495, L43
Gardiner L. T., Sawa T., Fujimoto M., 1994, MNRAS, 266, 567
Geha M. C. et al., 1998, AJ, 115, 1045
Geisler D., 1996, AJ, 111, 480
Geisler D., Sarajedini A., 1999, AJ, 117, 308
Geisler D., Bica E., Dottori H., Clariá J. J., Piatti A. E., Santos J. F. C., Jr, 1997, AJ, 114, 1920
Geisler D., Piatti A. E., Bica E., Clariá J. J., 2003, MNRAS, 341, 771
Girardi L., Bertelli G., Bressan A., Chiosi C., Groenewegen M. A. T., Marigo P., Salasnich B., Weiss A., 2002, A&A, 391, 195
Glatt K. et al., 2008a, AJ, 135, 1106
Glatt K. et al., 2008b, AJ, 136, 1703
Glatt K., Grebel E. K., Koch A., 2010, A&A, 517, A50
Gratton R. G., Ortolani S., 1988, A&AS, 74, 299
Hesser J. E., Warris W. E., vandenBerg D. A., Allwright J. W. B., Sholt P., Stetson P. B., 1987, PASP, 99, 39
Hodge P. W., 1986, PASP, 98, 1113
Hodge P. W., Wright F. W., 1974, AJ, 79, 858
Holtzman J. A. et al., 1997, AJ, 113, 656
Ibata R. A., Lewis G. F., Beaulieu J.-P., 1998, ApJ, 509, L29
Kallivayalil N., Patten B. M., Marengo M., Alcock Ch., Werner M. W., Fazio G. G., 2006, ApJ, 652, 1213
Kerber L. O., Girardi L., Rubele S., Cioni M. R., 2009, A&A, 499, 697
Lauberts A., 1982, ESO/Uppsala Survey of the ESO (B) Atlas. European Southern Observatory, Garching bei Munchen
Lejeune T., Schaerer D., 2001, A&A, 366, 538
Lindsay E. M., 1958, MNRAS, 118, 172
Mighell K. J., Sarajedini A., French R. S., 1998, AJ, 116, 2395 (MSF)
Murai T., Fujimoto M., 1980, PASJ, 32, 581
Pagel B. E. J., Tautvaišiene G., 1998, MNRAS, 299, 535
Parisi M. C., Grocholski A. J., Geisler D., Sarajedini A., Clariá J. J., 2009, AJ, 138, 517
Piatek S., Pryor C., Olszewski E. W., 2008, AJ, 135, 1024
Piatti A. E., 2010, A&A, 513, L13
Piatti A. E., Geisler D., Bica E., Clariá J. J., Santos J. F. C., Jr, Sarajedini A., Dottori H., 1999, AJ, 118, 2865
Piatti A. E., Santos J. F. C., Jr, Clariá J. J., Bica E., Sarajedini A., Geisler D., 2001, MNRAS, 325, 792
Piatti A. E., Sarajedini A., Geisler D., Bica E., Clariá J. J., 2002, MNRAS, 329, 556
Piatti A. E., Clariá J. J., Ahumada A. V., 2003a, MNRAS, 340, 1249
Piatti A. E., Geisler D., Bica E., Clariá J. J., 2003b, MNRAS, 343, 851
Piatti A. E., Bica E., Geisler D., Clariá J. J., 2003c, MNRAS, 344, 965
Piatti A. E., Clariá J. J., Ahumada A. V., 2003d, MNRAS, 346, 390
Piatti A. E., Clariá J. J., Ahumada A. V., 2004a, A&A, 418, 979
Piatti A. E., Clariá J. J., Ahumada A. V., 2004b, A&A, 421, 991
Piatti A. E., Santos J. F. C., Jr, Clariá Bica E., Ahumada A. V., Parisi M. C., 2005a, A&A, 440, 111
Piatti A. E., Sarajedini A., Geisler D., Seguel J., Clark D., 2005b, MNRAS, 358, 1215
Piatti A. E., Sarajedini A., Geisler D., Clark D., Seguel J., 2007a, MNRAS, 377, 300

Piatti A. E., Sarajedini A., Geisler D., Gallart D., Wischnjewsky M., 2007b, MNRAS, 381, L84
Piatti A. E., Sarajedini A., Geisler D., Gallart D., Wischnjewsky M., 2007c, MNRAS, 382, 1203
Piatti A. E., Geisler D., Sarajedini A., Gallart C., Wischnjewsky M., 2008, MNRAS, 389, 429
Piatti A. E., Geisler D., Sarajedini A., Gallart C., 2009, A&A, 501, 585
Piatti A. E., Clariá J. J., Parisi M. C., Ahumada A. V., 2011, PASP, in press
Rafelski M., Zaritsky D., 2005, AJ, 129, 2701
Rich R. M., Shara M., Fall M., Zurek D., 2000, AJ, 119, 197
Robertson B., Bullock J. S., Font A. S., Johnston K. V., Hernquist L., 2005, ApJ, 632, 872
Rochau B., Gouliermis D. A., Brandner W., Dolphin A. E., Henning T., 2007, ApJ, 664, 322
Sales L. V., Navarro J. F., Abadi M. G., Steinmetz M., 2007, MNRAS, 379, 1464
Schlegel D. J., Finkbeiner D. P., Davis M., 1998, ApJ, 500, 525 (SFD)
Searle S., Zinn R., 1978, ApJ, 225, 357
Stetson P. B., Davis L. E., Crabtree D. R., 1990, in Jacoby G., ed., ASP Conf. Ser. Vol. 8, CCDs in Astronomy. Astron. Soc. Pac., San Francisco, p. 289
Tsujimoto T., Bekki K., 2010, ApJ, 700, L69
Zaritsky D., Lin D. N. C., 1997, AJ, 114, 2545
Zentner A. R., Bullock J. S., 2003, ApJ, 598, 49

SUPPORTING INFORMATION

Additional Supporting Information may be found in the online version of this article:

Tables 2–15. CCD CT_1T_2 data of stars in the fields of the 14 clusters.

Please note: Wiley-Blackwell are not responsible for the content or functionality of any supporting materials supplied by the authors. Any queries (other than missing material) should be directed to the corresponding author for the article.

This paper has been typeset from a TEX/LATEX file prepared by the author.